

Available online at BCREC website: https://bcrec.id

BCREC

Bulletin of Chemical Reaction Engineering & Catalysis, 18 (4) 2023, 593-603

Research Article

Ag-TiO₂ for Efficient Methylene Blue Photodegradation Under Visible Light Irradiation

Hendri Widiyandari^{1,2,*}, Muhammad Nashir¹, Hanaiyah Parasdila¹, Khanza Fadhilah Almas¹, Risa Suryana¹

¹Department of Physics, Faculty of Mathematics and Natural Science, Sebelas Maret University, Jl. Ir. Sutami 36A Surakarta, Central Java, 57126, Indonesia. ²Centre of Excellence for Electrical Energy Storage Technology, Sebelas Maret University, Jl. Slamet Riyadi 435, Surakarta, Central Java 57146, Indonesia.

Received: 11st August 2023; Revised: 18th October 2023; Accepted: 19th October 2023 Available online: 23rd October 2023; Published regularly: December 2023



Abstract

Photocatalysis is one of the environmentally friendly methods for degrading down wastewater contamination. TiO_2 as one of the photocatalyst material is claimed can enhance the photocatalytic activity much better, if the band gap energy is reduced. In order to reduce the bandgap energy of TiO_2 , the novel in this research is that the temperature variations over a 24-hour period at 100 °C, 120 °C, 140 °C, and 160 °C in hydrothermal process to synthesize the photocatalyst material with Ag-doped. Diffraction patterns of Ag- TiO_2 show that all sample have tetragonal crystal structure and an anatase phase which also has excellent crystallinity. Some of the nanoparticles on the surface of Ag- TiO_2 have a consistent morphology, while other particles are formed irregularly. According to the DRS UV-Vis result, bandgap energy reduced as temperature increased (Eg = 3.2 eV to 2.32 eV). The results from PL Ag- TiO_2 160 have the lowest intensity, which indicates a low rate of electron-hole recombination. The Ag- TiO_2 160 sample produced the best photocatalytic activity, according to the results of the MB degradation test, with a relative change in concentration of 92.98% for 2 h under visible light.

Copyright © 2023 by Authors, Published by BCREC Group. This is an open access article under the CC BY-SA License (https://creativecommons.org/licenses/by-sa/4.0).

Keywords: Photocatalyst; Ag-TiO2; Temperature; Hydrothermal

How to Cite: H. Widiyandari, M. Nashir, H. Parasdila, K.F. Almas, R. Suryana (2023). Ag-TiO₂ for Efficient Methylene Blue Photodegradation Under Visible Light Irradiation. Bulletin of Chemical Reaction Engineering & Catalysis, 18(4), 593-603 (doi: 10.9767/bcrec.19885)

Permalink/DOI: https://doi.org/10.9767/bcrec.19885

1. Introduction

Chemical dyes are one of the many raw materials used in the textile industry. The environment loses over 700.000 tons of synthetic dyes annually worldwide [1]. Toxic substance of wastewater, particularly that containing dyes, has recently taken center stage in discussions about environmental sustainability. Conventional methods to dealing with water waste contamination, such as chemical oxidation, physical adsorption, and biological degradation, might be

difficult to execute and may still lead to the production of hazardous and pricey substances [2]. Therefore, we must substitute methods that can safely degrade organic contaminants at an affordable price. The technology is photocatalysis, this process utilizes among the most advanced oxidation methods to degrade organic contaminants, and it is reliant on semiconductor materials [3].

Specific environmentally beneficial metal oxide semiconductor materials, such as TiO₂, SnO₂, and ZnO, have excellent photocatalytic properties for effectively degrading organic contaminants [4]. In comparison to other semicon-

Email: hendriwidiyandari@staff.uns.ac.id (H. Widiyandari)

^{*}Corresponding Author.

ductor materials, TiO₂ offers various benefits, including chemical qualities that are stable, non-toxic, budget-friendly, and environmentally beneficial [5]. The possibility of using titanium dioxide (TiO₂) as a photocatalyst material for pollutant degrading applications has recently come under consideration. Its superior photocatalytic capabilities and corrosion resistance are to held responsible. The three primary crystal formations of TiO₂ are tetragonal anatase, rutile, and brookite (orthorhombic). Anatase has the best photocatalytic activity among the three crystalline forms of TiO₂ [6,7].

TiO₂ has a 3.0 eV to 3.2 eV broad bandgap energy. If TiO2 is only applied to ultraviolet (UV) light, which has a wavelength of 387 nm, its photocatalytic activities can still be active. Visible light is responsible for most of the sunlight reaching the Earth; ultraviolet light takes up relatively little of it. As a result, it will reduce the photocatalyst's capabilities. TiO2's capacity as a photocatalyst may be decreased by its rapid electron-hole recombination rate [8]. TiO2 can be doped with transition metals to boost its photocatalytic activity [9]. Consequently, it is anticipated that it may modify the capacity for absorbing light from the UV range to visible light. As a result, the photocatalytic activity will increase [10]. Barakat et al. [11] have been studied the effect of the temperature on the photocatalytic degradation of the rhodamine B dye with Ag-doped TiO2 nanofibers, it showed that temperature has positive impact on the photodegradation when the photocatalyst is exploited in the form of nanoparticles due to modification of the kinetic and the activation energies rather than the nanofiber. Singh et al. [12] have synthesized Ag-TiO₂ using wet chemical reaction. The UV-Vis spectroscopy test revealed enhanced absorbance in the TiO₂ doped Ag. Methylene blue was used to examine the photocatalytic activity of Ag- TiO₂ after it had been exposed to visible light. Agphotocatalytic TiO2's efficiency was increased by 89.2% after being exposed to radiation for a single hour. Compared to TiO2, its efficiency increased by almost 1.7 times. The decreased recombination of the electron-hole charges in TiO2 is the reason of the enhanced photocatalytic activity.

Compare to wet chemical reaction process, we conduct an experiment with hydrothermal methods to produce TiO₂ with nanoparticle morphology. Because hydrothermal method is relatively affordable to conduct a low crystallization temperature [13]. Water serves as the precursor solution in the hydrothermal process, which is beneficial to the environment because

the reaction occurs in a closed system. By varying the experimental variables, hydrothermal synthesis methods can efficiently control the yield of crystals formed. Temperature, pressure, time spent in the process, and concentration are just some of the experimental parameters [14]. TiO₂ was produced hydrothermally by Malligavathy et al. [15] at temperatures of 100 °C, 120 °C, 140 °C, and 160 °C. Results confirmed that TiO2's crystallinity and photocatalytic activity were affected by the hydrothermal temperature. The optimum photocatalytic activity has been identified in TiO₂, which was produced at 160 °C. For the degradation of rhodamine, the largest known degradation efficiency is 92.5%. Therefore, in this research, Ag-TiO₂ was synthesized via a hydrothermal method with various temperatures. This research's aim is to establish whether Agmicrostructure, TiO₂'s morphology, optical characteristics, and photocatalytic activity are influenced by hydrothermal temperature.

2. Materials and Methods

For sample preparation, silver nitrate (AgNO₃) (Merck, Indonesia), sodium hydroxide (NaOH) (Merck, Indonesia), and distilled water were mixed along with titanium (IV) isopropoxide Ti[OCH(CH₃)₂]₄ (Sigma-Aldrich 97%, Germany) without any further purification. A 10 ppm concentration of methylene blue (MB) is used as a dye for the degradation test.

An amount of 2 mL of titanium (IV) isopropoxide Ti[OCH(CH₃)₂]₄ was collected in a beaker and 20 mL of distilled water was added. The mixture was stirred with a magnetic stirrer for 3 h at room temperature with 2 mot rotation speed, and after that about 1-2 mL of AgNO₃ and NaOH were added while the solution was stirred until the solutions reached the pH 7 at 30 min. The reaction solution was then placed into an autoclave made of stainless steel and Teflon. After being placed in the furnace, the autoclave was heated for 24 h at various temperatures: 100 °C, 120 °C, 140 °C, and 160 °C. After heating process, the autoclave was cooled at room temperature and the resulting solution was washed with distilled water 3 times. Followed by drying the sample in an oven at 100 °C for 3 h and annealed for 5 h at 400

XRD (Bruker AXS D8 Advance X-Ray), SEM-EDX (JEOL JSM-6510LA), UV-Vis DRS (MAYA Pro2000 from Ocean Optics), Photoluminescence (PL) (Perkin Elmer LS 55), and a spectrophotometer were applied in order to characterize the material. (Perkin Elmer's

Lambda 25) UV-Vis. The purpose of XRD characterization is to identify the Ag- TiO₂'s crystal size or crystallinity level. The Ag- TiO₂ material was characterized using SEM-EDX to determine its surface morphology and particle size. The purpose of UV-Vis DRS characterization is to determine the sample's bandgap energy (Eg) and light absorption. To determine the material's rate of electron-hole recombination, PL was examined. The absorbance (A) of the MB solution was determined using a UV-Vis spectrophotometer before and after irradiation.

The photocatalytic activity test of the Ag-TiO₂ have been using the methylene blue (MB) dye model compound. Ag-TiO2 samples were weighed up to 100 mg and mixed with 50 cm³ of 10 ppm methylene blue for each temperature variations. The solution was first tested for absorption for 30 min without radiation. After that, this solution was irradiated to visible light for 120 min to examine for MB degradation. Radiation in a degradation test using a solar simulator (Peccel/PEC-L01) as the visible light source. The sample is located 13 cm from the lamp source. Centrifugation was used to separate the methylene blue solution from the Ag-TiO₂ powder in each sample of the solution that was tested for degradation. Using a UV-Vis spectrophotometer, the concentration of the degraded methylene blue solution was determined.

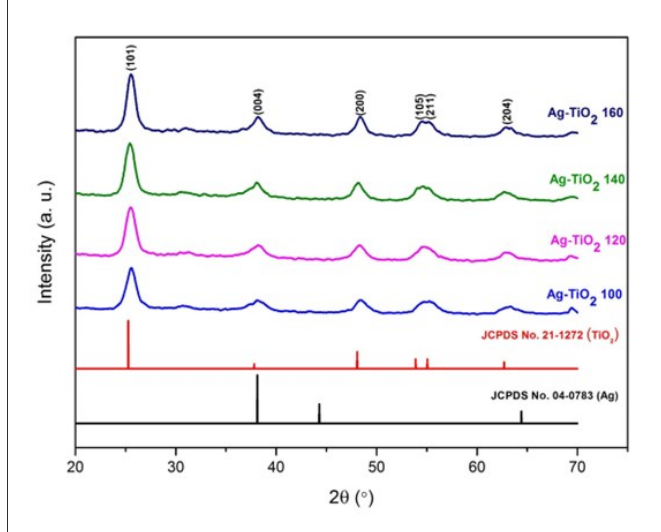


Figure 1. X-Ray diffraction pattern of Ag-TiO₂ with temperature variations.

3. Results and Discussion

In Figure 1, the XRD results are shown. The peaks from the XRD results are in line with the reference data JCPDS No. 21-1272, according to the results of the diffraction pattern of Ag-TiO₂. The following patterns have a tetragonal crystal structure and are in the anatase phase: (101), (004), (200), (105), (211), and (204). Also, the appearance of the peak (101) with the highest strength in the plane suggests that the synthesized TiO₂ crystals solely indicate the anatase phase. The low Ag concentration in Figure 1 prevents direct observation of the diffraction peak of Ag, which overlaps with roughly $2\theta = 38^{\circ}$. It is possible, according to these studies [16,17], for Ag nanoparticles to emerge at the crystal boundary and bond to the surface of TiO₂ crystals. Moreover, the peak of (111) Ag at (38.1°) is obscured because the diffraction peak of the Ti (004) plane is too high at (37.9°) [18,19].

Based on Figure 1, it can be seen that for the four samples, the intensity of the anatase peaks increases as the hydrothermal temperature increases. This indicates that crystallinity has increased and crystal formation has improved. Anatase TiO₂ crystals can form at the lowest temperature variation in our research, which is 100 °C. The Ag-TiO₂ 160 sample showed the finest crystallinity because the peak intensity was the highest. The Scherrer equation can be used to calculate the Ag-TiO₂ crystallite size (equation (1)). Only the anatase peaks were used to calculate crystallite sizes (101). Table 1 shows the crystallite size results for a plane (101).

$$D = \frac{k\lambda}{\beta\cos\theta} \tag{1}$$

where, D = size of crystal diameter, λ = wavelength of radiation, θ = angle of diffraction of Bragg, β = width of peak FWHM, k = constant (0,9) [3]. It is significant that when the hydrothermal temperature increases, Ag-TiO₂ crystallite size improves. The Ag-TiO₂ 160 sample has the largest crystallite size, whereas the Ag-TiO₂ 100 sample has the smallest. This is due to the fact that crystal growth will improve as temperature increases.

Tabel 1. Crystallite sizes and lattice parameters of Ag-TiO₂ samples.

Sample	Crystallite size (nm)	a (Å)	c (Å)	c/a
Ag-TiO ₂ 100	4.36	3.754	9.446	2.516
$Ag-TiO_2$ 120	4.42	3.765	9.449	2.509
$Ag-TiO_2$ 140	5.01	3.775	9.488	2.513
Ag-TiO ₂ 160	5.73	3.759	9.425	2.507

Figures 2 (a)-(d), show the results of SEM images of $Ag\text{-}TiO_2$ samples with temperature variations. The results show that the surface of the samples holds both particles with irregular shapes and some nanoparticles with a uniform morphology. The existence of the sample's atomic or elemental composition is confirmed using EDX analysis. Table 2 shows the EDX results in the data. According to the EDX results shown in Table 2, the sample's mass and atomic numbers are Ti, O, and Ag. This proves that the required element, silver (Ag), the dopant, is present in all TiO_2 samples.

The TEM and HR-TEM images of Ag-TiO₂ samples heated hydrothermally at 120 °C and 160 °C are shown in Figure 3. The TEM images of Ag-TiO₂ synthesized at 120 °C and 160 °C are shown in Figure 3, and they clearly depict monodispersed particles. Black colored spots on the TiO₂ surface illustrate the distribution of Ag. It can be observed that they have a relatively irregular particle shape and some showed a slight agglomeration [20]. At 120 °C, the majority of the Ag-TiO₂ particle sizes appeared to be between 4-6 nm. It correlates the crystallite size determined by XRD measure-

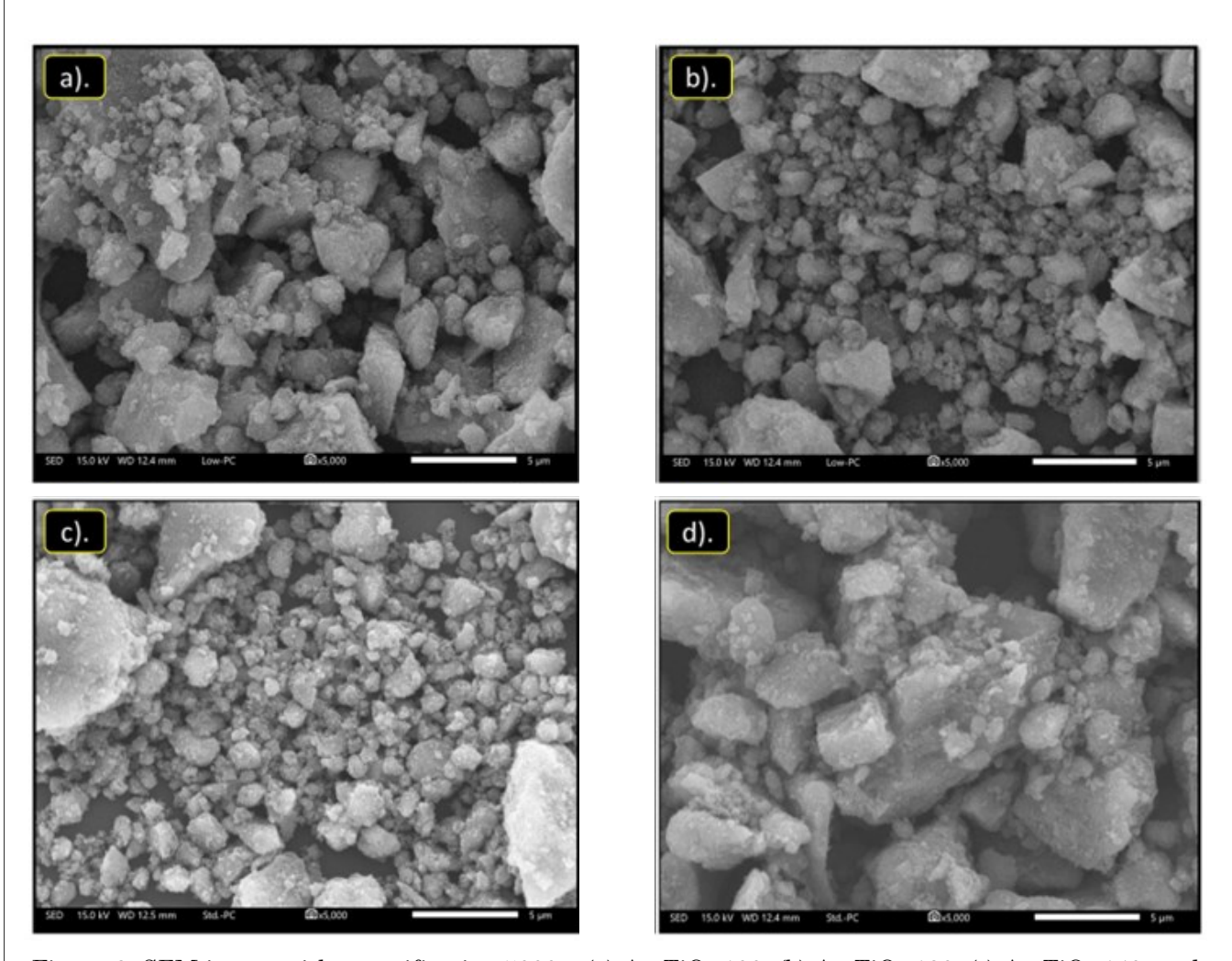


Figure 2. SEM image with magnification 5000x: (a) Ag-TiO₂ 100, (b) Ag-TiO₂ 120, (c) Ag-TiO₂ 140, and (d) Ag-TiO₂ 160.

Table 2. Atomic mass percentage of Ag-TiO₂ determined by EDX.

Sample	Mass (%)			Atomic (%)		
	Ti	O	Ag	Ti	O	Ag
Ag-TiO ₂ 100	33.85	59.87	6.28	15.68	83.03	1.29
$\mathrm{Ag}\text{-}\mathrm{TiO}_2\ 120$	38.84	54.65	6.51	18.91	79.68	1.41
$Ag-TiO_2$ 140	27.74	43.47	4.58	13.79	64.69	1.01
Ag-TiO ₂ 160	38.06	55.53	5.78	18.30	79.94	1.23

ments. The Ag-TiO₂ sample's particle sizes at 160 °C were in the 10–13 nm range. Agglomeration of crystallites is the cause of the discrep-

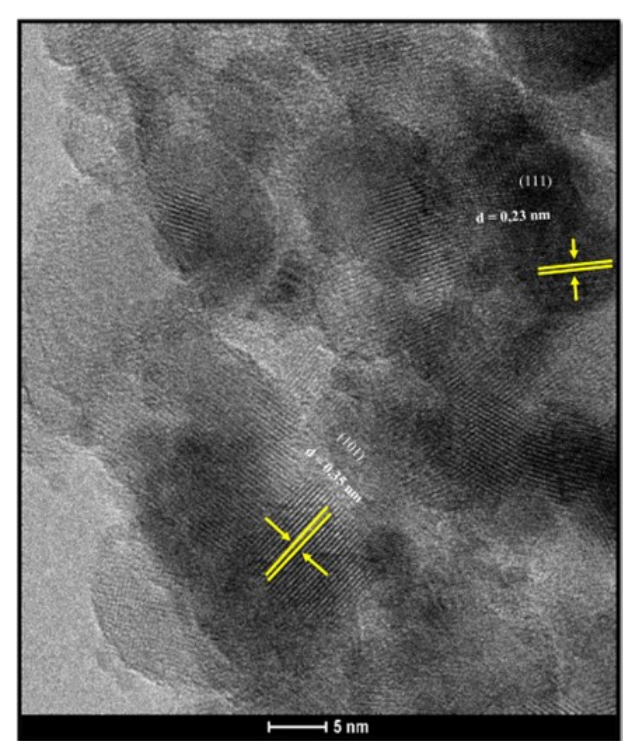


Figure 3. HR-TEM micrograph of sample Ag- TiO_2 160.

ancy between the particle size TEM and crystallite size XRD analyses at the Ag-TiO₂ 160 sample. Figure 3 also shows how the crystal's d-spacings are determined to be in the range of 0.35 nm, and 0.36 nm corresponds to the (101) plane of anatase TiO₂. Moreover, a 0.23 nm d-spacing crystal shall be considered, which matches the Ag's (111) plane. It shows that Ag is distributed uniformly across TiO₂. These planes are consistent with the XRD results [21,22].

Bandgap energy can be determined by the following Kubelka-Munk equation [23]:

$$F(R_{\infty}) = \frac{\left(1 - R_{\infty}\right)^2}{2R_{\infty}} = \frac{K}{S}$$
 (2)

where, $F\left(R_{\infty}\right)$ is the Kubelka-Munk function or the absolute reflectance of the sample, R_{∞} is the reflectance: Rsample/Rstandard, where K denotes the molar absorption scattering coefficient and S the coefficient constant. Tauc suggested analyzing optical absorption spectra to calculate the bandgap energy of semiconductors. The Tauc method is predicated on the notion of an energy-dependent absorption coefficient, which is denoted by the following equation [23]:

$$(\alpha hv)^{1/n} = (hv - Eg) \tag{3}$$

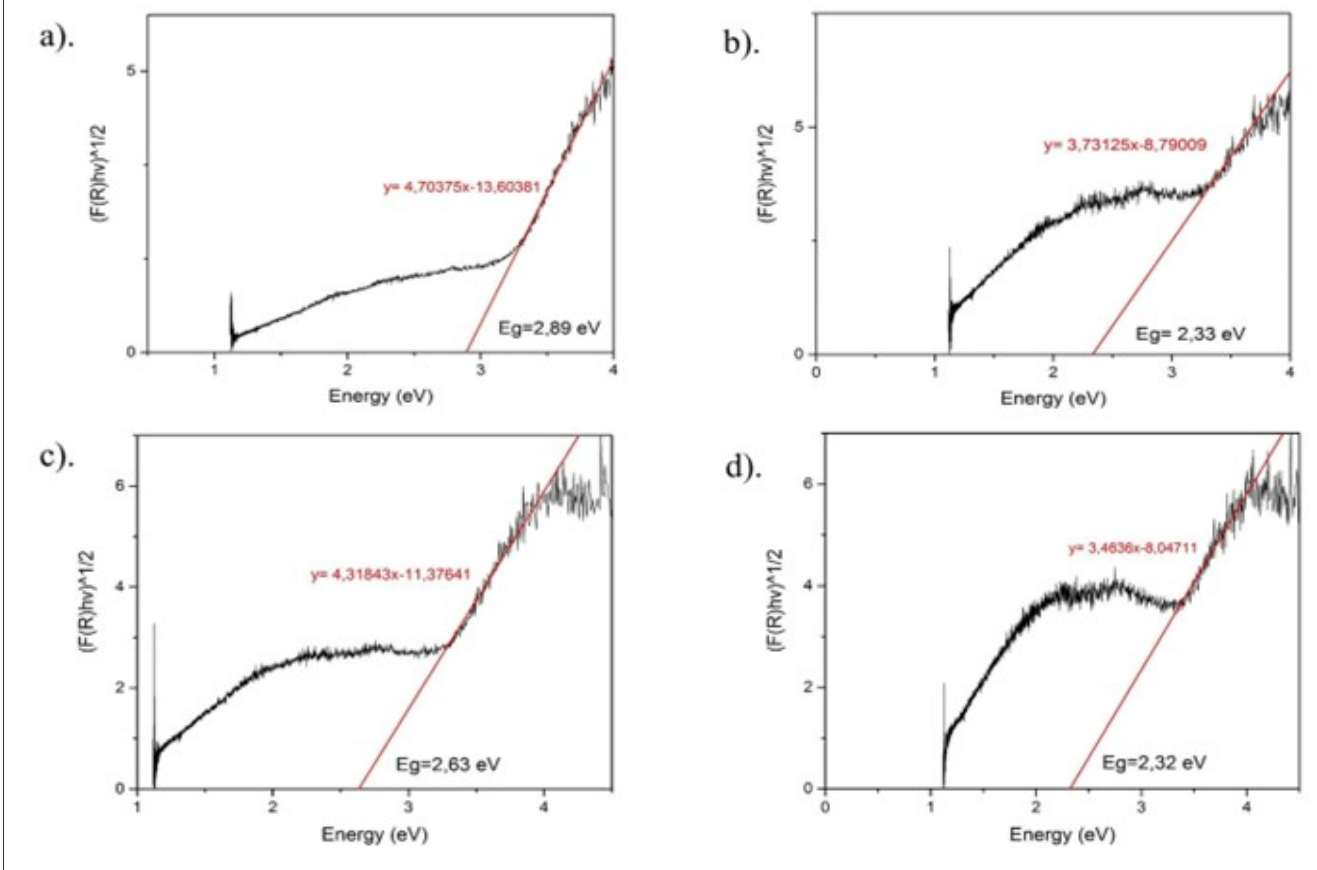


Figure 4. Bandgap energy: (a) Ag-TiO₂ 100, (b) Ag-TiO₂ 120, (c) Ag-TiO₂ 140, (d) Ag-TiO₂ 160.

Copyright © 2023, ISSN 1978-2993

thus,

$$\left[F(R_{\infty})hv\right]^{1/n} = A(hv - Eg) \tag{4}$$

where, the energy hu of the incident photon, E_g is the bandgap energy, A is the proportionality

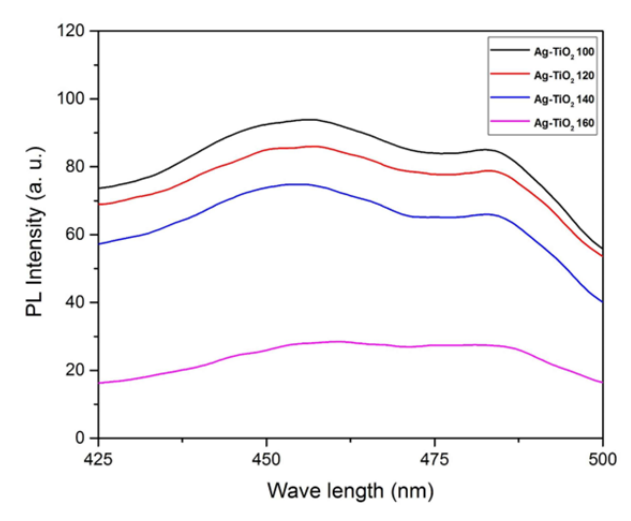


Figure 5. The PL Ag-TiO₂ spectrum with temperature variations.

constant and n is the constant type of electron transition. n for direct transitions is equal to 12, and n for indirect transitions is equal to 2. Plotting the graph of $[F\ (R)\ h]\ (1/n)$ vs the energy of the photons allows one to calculate the energy of the bandgap $Eg\ (hv)$. Figure 4 shows the graph between $[F\ (R)\ h]\ (1/2)$ vs h (eV), which shows how the Tauc plot method based on the Kubelka-Munk equation is used to calculate the sample's bandgap energy value. TiO_2 has a bandgap energy of 3.20 eV.

The gap energy value changes as a result of the added Ag doping and temperature. With an increase in temperature, the energy gap reduces by 2.89 eV, 2.33 eV, 2.63 eV, and 2.32 eV. It is also clear that the bandgap energy of Ag that has been doped with TiO₂ can lower the band gap energy of TiO₂, increasing TiO₂'s capacity to absorb light in the visible spectrum. Ag's specific surface plasmon resonance (LSPR) effect, which enhances in the absorption of visible light, seems to be to responsible for this [24]. With increasing temperatures, the bandgap's energy reduces.

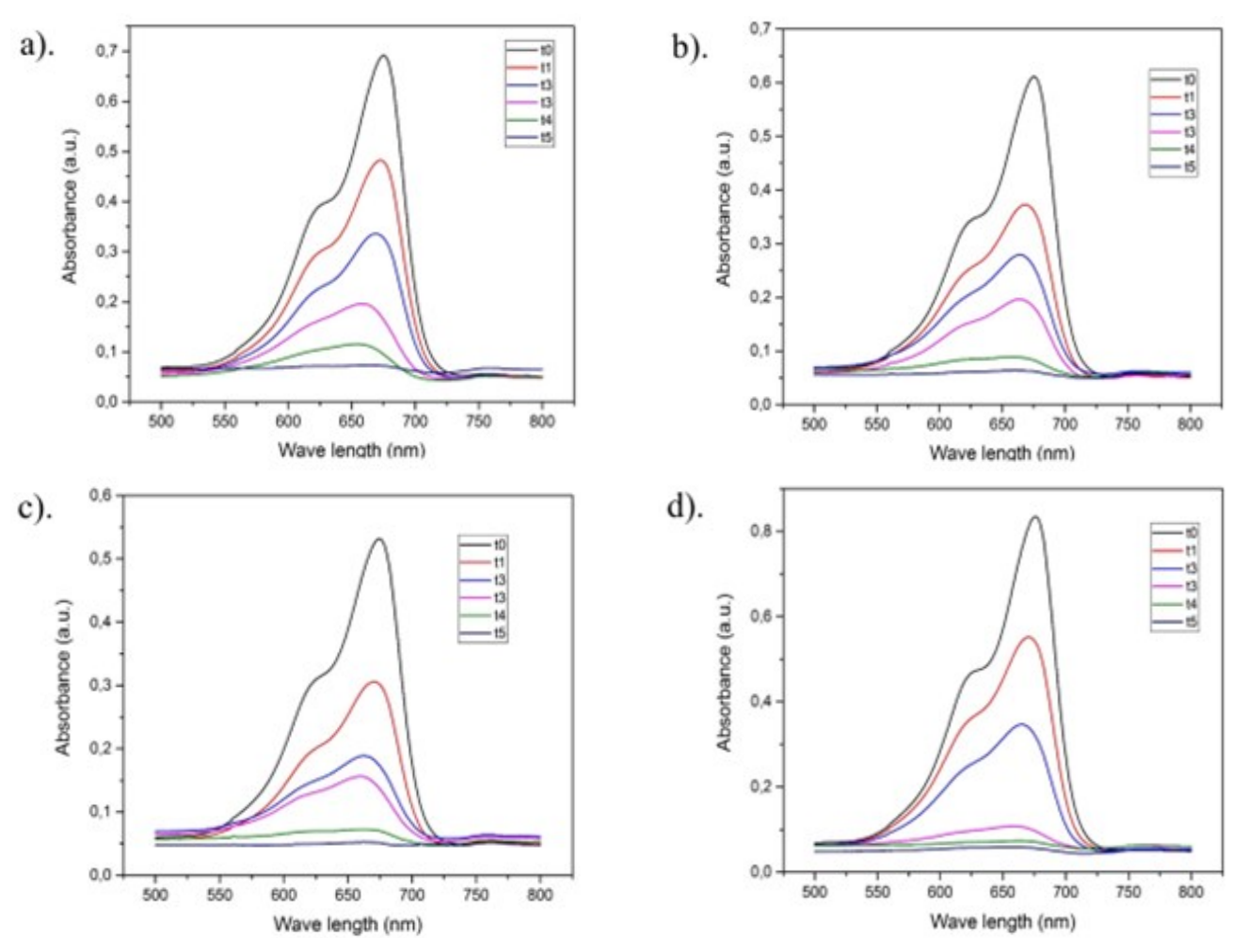


Figure 6. The absorbance spectrum of methylene blue with a radiation time of 120 min using samples: (a) Ag-TiO₂ 100, (b) Ag-TiO₂ 120, (c) Ag-TiO₂ 140, (d) Ag-TiO₂ 160.

The bandgap's energy value decreased from Ag-TiO₂ 100 to Ag-TiO₂ 120, increased from Ag-TiO₂ 120 to Ag-TiO₂ 140, and then decreased from Ag-TiO₂ 140 to Ag-TiO₂ 160. The transfer of charge between the Ag metal's electrons in the d energy level and the TiO₂ valence band, which causes the bandgap to shorten, is responsible for the bandgap's decrease. Because of this, the Ag nanoparticles shift the electronic state of TiO₂ in a way that prevents charge recombination and allows excited electrons from the valence band to be absorbed [25]. The Ag-TiO₂ 160 sample has the least bandgap energy value, measuring 2.3 eV.

Figure 5 shows the Ag-TiO₂ samples' photoluminescence spectrum. This spectrum is used to examine electron-hole pairs that form as a result of electron-hole recombination and produce PL emission in semiconductors. Although the PL intensity on Ag-TiO₂ 160 is the lowest, it can be seen that the emission peaks in the other Ag-TiO₂ samples are practically identical. The intensity PLreduces with increasing hydrothermal temperature. This decrease in intensity indicates a slow recombination rate.

Hence, it can improve how well electrons and holes are separated. The photocatalytic activity of the Ag-TiO₂ 160 sample is affected by the more effective electron-hole separation and lower recombination rate of this sample. The photocatalytic activity of TiO₂ is successfully reduced by the addition of Ag via minimizing electron-hole pair recombination [26].

Methylene blue (MB) compounds were used to examine Ag-photocatalytic TiO₂'s activity at various temperatures, through the use of photodegradation, this test is conducted by light from a solar simulator (visible light source). The absorbance of the UV-Vis results for all variations of the Ag-TiO₂ sample are shown in Figure 6. The decolorization change of methylene blue in the Ag-TiO₂ samples can be seen in Figure 7.

The degradation efficiency of the dye is calculated using the following formula:

Efficiency (%) =
$$\frac{\left(A_0 - A\right)}{A_0} \times 100\%$$
 (5)

where, A_0 and A are the absorbance of the dye solution before and after irradiation for time t, respectively [14].

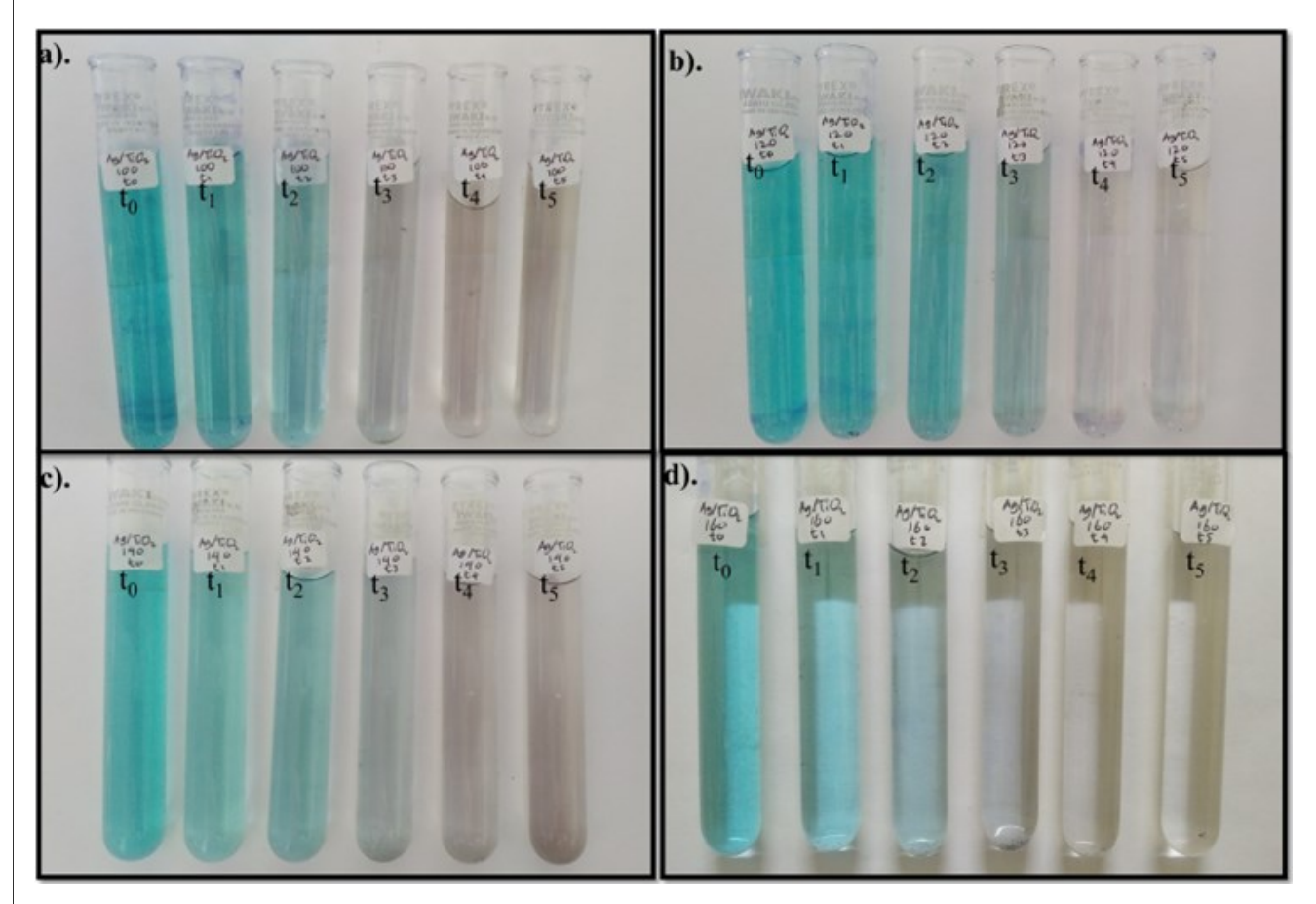


Figure 7. Coloration change of methylene blue in samples: a). Ag- TiO_2 100, b). Ag- TiO_2 120, c). Ag- TiO_2 140, and d). Ag- TiO_2 160.

Figure 8 shows the degradation efficiency. It is clear that the Ag-TiO₂ 160 sample has the optimum performance, reaching in at about 92.98%. In terms of comparison, the Ag-TiO₂ 160 sample exhibits the highest level of photocatalytic activity. These results back up the hypothesis that increasing the heating temperature can enhance photocatalytic activity. This result contributes to hypothesis that the shortest bandgap value of sample Ag-TiO₂ 160effects photocatalytic process and by having a lower PL intensity than other samples. Thus, a decrease in the recombination rate indicates an increase in the efficiency of the separation of the resultant electrons and holes. Furthermore, the presence of Ag ions successfully reduces the recombination of disadvantageous electron-hole pairs, resulting in more free charge carriers involved in the photocatalytic activity on the TiO₂ surface. The Ag-TiO₂ 160 also sample has the largest crystal size, indicating the best crystallinity, it comes from the increased temperature, increased crystallinity, larger crystal size, increased surface area, and the presence of the anatase phase [14].

The rate kinetics of the MB photocatalytic degradation were calculated using a first-order reaction kinetics model as given in the following equation [27,28]:

$$\ln\left(\frac{C_0}{C_t}\right) = kt

\tag{6}$$

The rate constant, k (min⁻¹), is calculated from the slope ln (C_0/C_t) versus the time (t) where C_0 is the initial concentration of methylene blue, Cis the concentration of methylene blue at different irradiation time [29]. The results of the kinetics graph of the rate of the photocatalytic

100 - Without Ag-TiO₂
Ag-TiO₂ 100
- Ag-TiO₂ 120
- Ag-TiO₂ 140
- Ag-TiO₂ 160

80 - Ag-TiO₂ 160

Time (minute)

Figure 8. The percentage degradation of MB.

degradation of MB by the Ag-TiO₂ samples are shown in Figure 9. Then the rate constants (k, min⁻¹) of degradation were obtained as follows: 0.01917; 0.01901; 0.01962; 0.02396 for samples Ag-TiO₂ 100, Ag-TiO₂ 120, Ag-TiO₂ 140, Ag-TiO₂ 160, respectively. The degradation reaction rate of MB dye degradation by Ag-TiO₂ 160 samples was the fastest compared to other samples. The results of the reaction rate kinetics are also following the percentage of degradation of the MB.

Ag-TiO₂ is irradiated with visible light, which excites the electrons in the valence band to the conduction band and leaves a hole in the valence band. This is one of the photocatalytic mechanisms for MB degradation. The silver absorbs the electrons that were excited to the TiO₂ conduction band. The quick transmission of excited, high-energy electrons from the TiO₂ conduction band to the metal is improved by Ag-TiO₂ structure. The primary goal is to and minimize electron-hole prevent recombination, and Ag will react as electron traps to enhance the durability of the electrons [30].

The oxygen molecule that has been absorbed on the surface of TiO2 will absorb the released electrons from Ag, which will then undertake further reduction to form superoxide radicals (\cdot O₂-) [31,32]. In order to create (HOO •), hydroperoxy radicals hydroxylated next. H₂O₂ is formed when the hydroxyl radical (OH) and the trapped electrons interact. Hydroxyl radicals (OH), which are very active for degradation, are produced by the holes in the valence band when they interact with water adsorbed on the surface. The methylene blue is degraded by these reactive molecules reacting with hydrox-

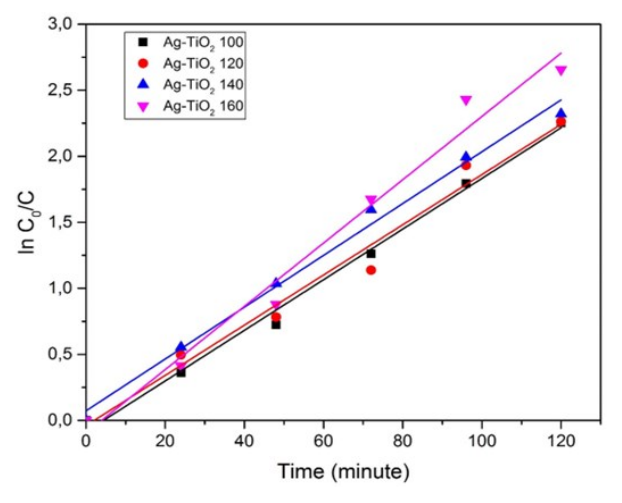


Figure 9. Graph of the kinetics rate degradation of the Ag-TiO₂.

yl radicals (OH) went through undergoes demethylation resulting in the formation of some intermediate products such as (Azure A, Azure B, Azure C, and Thionin), and the final degraded products are CO₂ and H₂O [33–35].

4. Conclusion

Hydrothermal temperature variations can improve the physical and photocatalytic properties of Ag-TiO2 samples. Ag-TiO2 160 produced crystals with a higher level of crystallinity will grow larger as the heating temperature increases. Temperature increases also result in larger crystals. When the hydrothermal temperature increases, the rate of electron-hole recombination reduces, enhancing the effectiveness of electron-hole separation. The Ag-TiO₂ 160 sample had the remarkable photocatalytic activity, with an MB degradation efficiency of 92.98% during 120 minutes of visible light exposure. This can be taken into consideration for the mass manufacture of Ag-TiO2 to be applied as a material that degrades water pollutants using visible light, as one of the renewable energy sources.

Acknowledgement

This research was funded by The Ministry of Education, Culture, Research, and Technology Republic of Indonesia under the research grant of World Class Research with contract number 2104/UN27.22/PT.01.03/2021

CRediT Author Statement

Hendri Widiyandari: Conceptualization, Validation, Writing Original Methodology, Draft, Review & Editing; Muhammad Nashir: Validation, Investigation, Writing Original Draft, Data Collecting, Visualization; Hanaiyah Parasdila: Writing, Review & Editing; Khanza Fadhilah Almas: Investigation, Visualization, Writing, Review & Editing; Risa Suryana: Writing, Review & Editing.

References

[1] Al-Mamun, M.R., Kader, S., Islam, M.S., Khan, M.Z.H. (2019). Photocatalytic activity improvement and application of UV-TiO2 photocatalysis in textile wastewater treatment: A review. *Journal of Environmental Chemical Engineering*, 7(5), 103248. DOI: 10.1016/j.jece.2019.103248.

- [2] Cao, X., Tao, J., Xiao, X., Nan, J. (2018). Hydrothermal-assisted synthesis of the multi-element-doped TiO₂ micro/nanostructures and their photocatalytic reactivity for the degradation of tetracycline hydrochloride under the visible light irradiation. *Journal of Photochemistry and Photobiology A: Chemistry*, 3 6 4, 2 0 2 2 0 7. D O I: 10.1016/j.jphotochem.2018.06.013.
- [3] Sarteep, Z., Pirbazari, A.E., Aroon, M.A. (2016). Silver doped TiO2 nanoparticles: preparation, characterization and efficient degradation of 2, 4-dichlorophenol under visible light. *Journal of Water and Environmental Nanotechnology*, 1(2), 135-144. DOI: 10.7508/jwent.2016.02.007.
- [4] Messih, M.A., Ahmed, M.A., Soltan, A., Anis, S.S. (2019). Synthesis and characterization of novel Ag/ZnO nanoparticles for photocatalytic degradation of methylene blue under UV and solar irradiation. *Journal of Physics and Chemistry of Solids*, 135, 109086. DOI: 10.1016/j.jpcs.2019.109086.
- [5] Nasralla, N., Yeganeh, M., Astuti, Y., Piticharoenphun, S., Shahtahmasebi, N., Kompany, A., Karimipour, M., Mendis, B.G., Poolton, N.R.J., Šiller, L. (2013). Structural and spectroscopic study of Fe-doped TiO₂ nanoparticles prepared by sol-gel method. Scientia Iranica, 20(3), 1018-1022. DOI: 10.1016/j.scient.2013.05.017.
- [6] Khaki, M.R.D., Shafeeyan, M.S., Raman, A.A.A., Daud, W.M.A.W. (2017). Application of doped photocatalysts for organic pollutant degradation-A review. *Journal of environ*mental management, 198, 78-94. DOI: 10.1016/j.jenvman.2017.04.099.
- [7] Daghrir, R., Drogui, P., Robert, D. (2013). Modified TiO2 for environmental photocatalytic applications: a review. *Industrial & Engineering Chemistry Research*, 52(10), 3581-3599. DOI: 10.1021/ie303468t.
- [8] Padmanaban, A., Dhanasekaran, T., Kumar, S.P., Gnanamoorthy, G., Munusamy, S., Stephen, A., Narayanan, V. (2017). Visible light photocatalytic property of Ag/TiO2 composite. *Mechanics, Materials Science & Engi*neering Journal, 9(1), 01498142. DOI: 10.2412/mmse.97.67.748.
- [9] Liu, Z., Liu, X., Lu, Q., Wang, Q., Ma, Z. (2019). TiOF2/TiO2 composite nanosheets: Effect of hydrothermal synthesis temperature on physicochemical properties and photocatalytic activity. *Journal of the Taiwan Institute of Chemical Engineers*, 96, 214-222. DOI: 10.1016/j.jtice.2018.11.013.

- [10] Harikishore, M., Sandhyarani, M., Venkateswarlu, K., Nellaippan, T.A., Rameshbabu, N. (2014). Effect of Ag doping on antibacterial and photocatalytic activity of nanocrystalline TiO₂. Procedia Materials Science, 6, 557-566. DOI: 10.1016/j.mspro.2014.07.071.
- [11] Barakat, N.A., Kanjwal, M.A., Chronakis, I.S., Kim, H.Y. (2013). Influence of temperature on the photodegradation process using Ag-doped TiO₂ nanostructures: negative impact with the nanofibers. *Journal of Molecular Catalysis A: Chemical*, 366, 333-340. DOI: 10.1016/j.molcata.2012.10.012.
- [12] Singh, J., Tripathi, N., Mohapatra, S. (2019). Synthesis of Ag-TiO₂ hybrid nanoparticles with enhanced photocatalytic activity by a facile wet chemical method. *Nano-Structures* & *Nano-Objects*, 18, 100266. DOI: 10.1016/j.nanoso.2019.100266.
- [13] Lu, H., Zhou, Y., Vongehr, S., Tang, S., Meng, X. (2012). Effects of hydrothermal temperature on formation and decoloration characteristics of anatase TiO₂ nanoparticles. Science China Technological Sciences, 55, 894-902. DOI: 10.1007/s11431-011-4706-4.
- [14] Yu, J., Wang, G., Cheng, B., Zhou, M. (2007). Effects of hydrothermal temperature and time on the photocatalytic activity and microstructures of bimodal mesoporous TiO_2 powders. Applied Catalysis B: Environmental, 69(3-4), 171-180. DOI: 10.1016/j.apcatb.2006.06.022.
- [15] Malligavathy, M., Iyyapushpam, S., Nishanthi, S.T., Padiyan, D.P. (2018). Role of hydrothermal temperature on crystallinity, photoluminescence, photocatalytic and gas sensing properties of TiO₂ nanoparticles. Pramana, 90, 1-13. DOI: 10.1007/s12043-018-1533-1.
- [16] Avciata, O., Benli, Y., Gorduk, S., Koyun, O. (2016). Ag doped TiO2 nanoparticles prepared by hydrothermal method and coating of the nanoparticles on the ceramic pellets for photocatalytic study: Surface properties and photoactivity. Journal of Engineering Technology and Applied Sciences, 1(1), 34-50. DOI: 10.30931/jetas.281381.
- [17] Wang, S., Han, Z., Di, T., Li, R., Liu, S., Cheng, Z. (2019). Preparation of pod-shaped TiO₂ and Ag@TiO₂ nano burst tubes and their photocatalytic activity. *Royal Society Open Science*, 6(9), 191019. DOI: 10.1098/rsos.191019.

- [18] Li, S., Zhu, X., Wang, B., Qiao, Y., Liu, W., Yang, H., Liu, N., Chen, M., Haifei Lu, H., Yang, Y. (2018). Influence of Ag nanoparticles with different sizes and concentrations embedded in a TiO₂ compact layer on the conversion efficiency of perovskite solar cells. *Nanoscale Research Letters*, 13, 1-11. DOI: 10.1186/s11671-018-2626-y.
- [19] Zhang, Y., Fu, F., Li, Y., Zhang, D., Chen, Y. (2018). One-step synthesis of Ag@ TiO₂ nanoparticles for enhanced photocatalytic performance. *Nanomaterials*, 8(12), 1032. DOI: 10.3390/NANO8121032.
- [20] Rao, T.N., Babji, P., Ahmad, N., Khan, R.A., Hassan, I., Shahzad, S.A., Husain, F.M. (2019). Green synthesis and structural classification of Acacia nilotica mediated-silver doped titanium oxide (Ag/TiO₂) spherical nanoparticles: Assessment of its antimicrobial and anticancer activity. Saudi Journal of Biological Sciences, 26(7), 1385-1391. DOI: 10.1016/j.sjbs.2019.09.005.
- [21] Desiati, R.D., Taspika, M., Sugiarti, E. (2019). Effect of calcination temperature on the antibacterial activity of TiO₂/Ag nanocomposite. *Materials Research Express*, 6(9), 095059. DOI: 10.1088/2053-1591/ab155c.
- [22] Suwarnkar, M.B., Dhabbe, R.S., Kadam, A.N., Garadkar, K.M. (2014). Enhanced photocatalytic activity of Ag doped TiO₂ nanoparticles synthesized by a microwave assisted method. *Ceramics International*, 40(4), 5489-5496. DOI: 10.1016/j.ceramint.2013.10.137.
- [23] da Silva Sousa, G., Nobre, F.X., Júnior, E.A.A., Sambrano, J.R., dos Reis Albuquerque, A., dos Santos Bindá, R., da Costa Couceiro, P.R., Brito, W.R., Cavalcante, L.S., de Morais Chaves Santos, M.R., de Matos, J.M.E. (2020). Hydrothermal synthesis, structural characterization and photocatalytic properties of β-Ag₂MoO₄ microcrystals: correlation between experimental and theoretical data. Arabian Journal of Chemistry, 13(1), 2 8 0 6 2 8 2 5 . D O I : 10.1016/j.arabjc.2018.07.011.
- [24] Makuła, P., Pacia, M., Macyk, W. (2018). How to correctly determine the band gap energy of modified semiconductor photocatalysts based on UV-Vis spectra. The journal of physical chemistry letters, 9(23), 6814-6817. DOI: 10.1021/acs.jpclett.8b02892.
- [25] Leong, K.H., Gan, B.L., Ibrahim, S., Saravanan, P. (2014). Synthesis of surface plasmon resonance (SPR) triggered Ag/TiO₂ photocatalyst for degradation of endocrine disturbing compounds. *Applied Surface Science* 128-135. DOI: 10.1016/j.apsusc.2014.06.153.

- [26] Mosquera, A.A., Albella, J.M., Navarro, V., Bhattacharyya, D., Endrino, J.L. (2016). Effect of silver on the phase transition and wettability of titanium oxide films. *Scientific re*ports, 6(1), 32171. DOI: 10.1038/srep32171.
- [27] Komaraiah, D., Radha, E., Sivakumar, J., Reddy, M.R., Sayanna, R. (2020). Photoluminescence and photocatalytic activity of spin coated Ag+ doped anatase TiO₂ thin films. *Optical Materials*, 108, 110401. DOI: 10.1016/j.optmat.2020.110401.
- [28] Astuti, Y., Musthafa, F., Arnelli, A., Nurhasanah, I. (2022). French fries-like bismuth oxide: physicochemical properties, electrical conductivity and photocatalytic activity. Bulletin of Chemical Reaction Engineering & Catalysis, 17(1), 146-156. DOI: 10.9767/bcrec.17.1.12554.146-156.
- [29] Astuti, Y., Arnelli, A., Pardoyo, P., Fauziyah, A., Nurhayati, S., Wulansari, A. D., Andianingrum, R., Widiyandari, H., & Bhaduri, G. A. (2017). Studying impact of different precipitating agents on crystal structure, morphology and photocatalytic activity of bismuth oxide. Bulletin of Chemical Reaction Engineering & Catalysis, 12(3), 478-484. DOI: 10.9767/bcrec.12.3.1144.478-484.
- [30] Tien, N.T.C., Nhut, C.H., Thuy, V.T.T., Huyen, T.T.B., Hien, L.P.T., Huy, N.N. (2022). Enhancement in photocatalytic efficiency of commercial TiO2 nanoparticles by calcination: A case of doxycycline removal. Bulletin of Chemical Reaction Engineering & Catalysis, 17(3), 486-496. DOI: 10.9767/bcrec.17.3.13970.486-496.

- [31] Bassim, S., Mageed, A.K., AbdulRazak, A.A., Al-Sheikh, F. (2023). Photodegradation of Methylene Blue with Aid of Green Synthesis of CuO/TiO₂ Nanoparticles from Extract of Citrus Aurantium Juice. Bulletin of Chemical Reaction Engineering & Catalysis, 18(1), 1-16. DOI: 10.9767/bcrec.16417.
- [32] Li, W., Xie, L., Zhou, L., Ochoa-Lozano, J., Li, C., Chai, X. (2020). A systemic study on Gd, Fe and N co-doped TiO₂ nanomaterials for enhanced photocatalytic activity under visible light irradiation. *Ceramics International*, 46(15), 24744-24752. DOI: 10.1016/j.ceramint.2020.06.265.
- [33] A Jawad, A. H., Mubarak, N.S.A., Ishak, M. A.M., Ismail, K., Nawawi, W.I. (2016). Kinetics of photocatalytic decolourization of cationic dye using porous TiO₂ film. *Journal of Taibah University for Science*, 10(3), 352-362. 2016, DOI: 10.1016/j.jtusci.2015.03.007.
- [34] Chen, Z., Fang, L., Dong, W., Zheng, F., Shen, M., Wang, J. (2014). Inverse opal structured Ag/TiO₂ plasmonic photocatalyst prepared by pulsed current deposition and its enhanced visible light photocatalytic activity. *Journal of Materials Chemistry A*, 2(3), 824-832. DOI: 10.1039/c3ta13985a.
- [35] Rauf, M.A., Meetani, M.A., Khaleel, A., Ahmed, A. (2010). Photocatalytic degradation of methylene blue using a mixed catalyst and product analysis by LC/MS. Chemical Engineering Journal, 157(2-3), 373-378. DOI: 10.1016/j.cej.2009.11.017